ISSN 0915-633X

NATIONAL INSTITUTE FOR FUSION SCIENCE

Kinetic Depletion Model for Pellet Ablation

Boris V. Kuteev

(Received - Oct. 10, 2001)

NIFS-716 Nov. 2001

RESEARCH REPORT
NIFS Series

TOKI, JAPAN

Kinetic Depletion Model for Pellet Ablation

Boris V. KUTEEV

State Technical University, St. Petersburg 195251, RUSSIA
National Institute for Fusion Science, Toki, Gifu 509-5292, JAPAN

e-mail: kuteev@phtf.stu.neva.ru

Keywords: pellet, ablation, kinetics, depletion, deceleration, toroidal effects

Abstract:

A kinetic model for depletion effect, which determines pellet ablation when the pellet passes a rational magnetic surface, is formulated. The model predicts a moderate decrease of the ablation rate compared with the earlier considered monoenergy versions [1, 2]. For typical T-10 conditions the ablation rate reduces by a factor of 2.5 when the 1-mm pellet penetrates through the plasma center. A substantial deceleration of pellets -about 15% per centimeter of low shire rational q region; is predicted.

Penetration for Low Field Side and High Field Side injections is considered taking into account modification of the electron distribution function by toroidal magnetic field. It is shown that Shafranov shift and toroidal effects yield the penetration length for HFS injection higher by a factor of 1.5. This fact should be taken into account when plasma-shielding effects on penetration are considered.

1 Introduction

The problem of the ablation heat flux self-limiting or depletion when pellet penetrates through a rational magnetic surface has been considered in Ref. [1-4]. The phenomenon developing as a significant reduction of the ablation rate near rational magnetic surfaces and the plasma center has been observed in many experiments [5,6]. The collisional limit of the problem has been considered in [7]. It was assumed that mixing the ablated and ambient plasmas affects the ablation rate. Qualitatively, that allowed getting a reduction of the ablation rate near rational surfaces. However, in contemporary tokamaks and stellarators the collisionless conditions for electrons are closer to reality. For a group of electrons with a definite energy the estimations of the effect was considered in Ref. [1]. It was assumed that the electrons leave the volume around the pellet with an average velocity reducing density of the group. The result gives asymptotic density decay varying with the interaction time t as $1/t$. This is incorrect because the energetic particle leave the finite volume at a finite time. A more detailed analysis accounting for the Maxwellian distribution of electrons was performed in Ref. [2-4]. As a result, the depletion was described in a quantitative manner and even allowed using the effect for diagnostics of the magnetic shear. However, the approach of Ref. [2-4] used a simplified averaging procedure and had a free parameter of the problem that is the cloud size, which allowed getting the results only by matching the solution at a point.

In this paper the problem is considered generally on kinetic basis. The depletion model is considered in Section 2. The pellet deceleration near rational magnetic surfaces is predicted. in a An example, illustrating numerical situation for T-10 conditions is presented in Section 3. In Section 4 toroidal effects on the pellet penetration from high field side and low field side are considered. A summary is given in Section 5.

2 Depletion Model

Let us consider a spherical pellet with radius r_p moving with velocity v_p across a rational magnetic surface with length L. At the plasma center $L=2\pi R$ where R is the major radius of the plasma. For safety factor $q=1$ the length is

almost the same $L=2\pi(R^2+r^2)^{1/2}$ when r is the minor radius of the magnetic surface.

Even for the thermal electrons with temperature about 1 keV these distances are much less than the mean free pass. Meanwhile, the ablation is defined by a tail of the electron distribution function with energies higher than (4-5) T_e [8]. This means that analyzing the depletion phenomenon one should consider the problem as strongly collisionless.

For this case, the problem is close to the classical problem dealing with one-dimensional expansion of finite-length gas cloud into vacuum [9]. The electron distribution function is defined by the Boltzmann collisionless equation

$$\frac{\partial}{\partial t}(nf)+v\cdot\frac{\partial}{\partial x}(nf)=0 \qquad (1)$$

We concern with application of this equation to initial problems for which

$$nf(v,x,t=0)=n_i\cdot f_i(v,x-vt) \qquad (2)$$

The solution of Eq. (1) is that nf remains constant along the molecular paths which are the characteristics of the equation

$$nf(v,x,t)=n_i\cdot f_i(v,x-vt) \qquad (3)$$

For our case the distiribution function f_i is Maxwellian and initial density n_i is a constant inside space interval $0<x<L$. This means that the distribution function at point $x=0$ will vary with time as the Maxwellian distribution with a cut tail beginning from the velocity

$$v=\frac{L}{y}v_p \qquad (4)$$

or the corresponding energy

$$E=\frac{m_e}{2}\left(\frac{L}{y}v_p\right)^2 \qquad (5)$$

Here y is the shadow distance between the point of first touching the closed magnetic surface and the projection of current point onto the normal to the magnetic field plane, which contains the pellet velocity vector v_p. (We assume for simplicity that the pellet velocity vector is also perpendicular to the magnetic field). Figure 1 shows the definitions as well as the distribution function at different values of y.

It is easy to calculate the electron *density* $n(0,t)$, the particle flow $\Gamma(0,t)$ and the heat flow $Q(0,t)$ at the border of the plasma and pellet cloud:

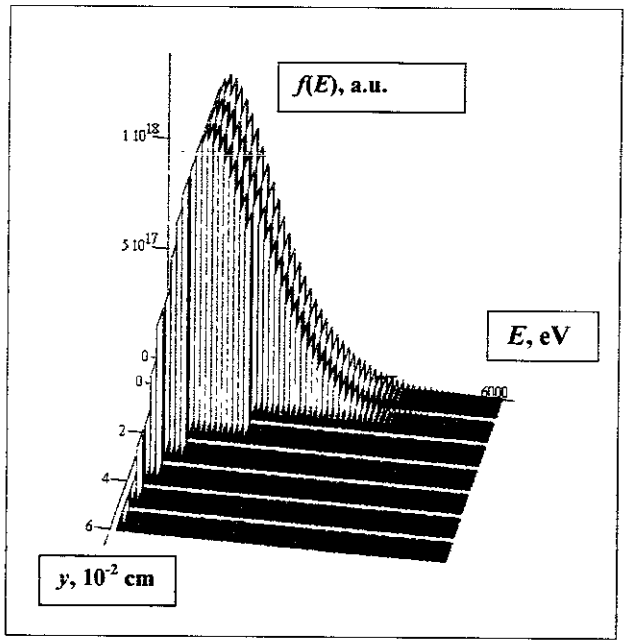

Figure 1: The evolution of the distribution function in the pellet shadow.

$$n(0,t)=\frac{n_i}{2}erf\left[2\beta\frac{L}{y}v_p\right]$$
$$\beta=(2RT_{e0})^{-1/2}, \qquad (6)$$
$$R=\frac{k}{m_i}$$

$$\Gamma(0,t)=\frac{n_i\cdot\beta}{2\cdot\pi^{1/2}}\left[1-exp\left(-4\beta^2\left(\frac{L}{y}v_p\right)^2\right)\right] \qquad (7)$$

$$Q(0,t)=\frac{1}{4}\cdot\frac{m_e}{\pi^{1/2}\cdot\beta^3}\left[1-\left(1+\beta^2\cdot\frac{L^2\cdot v_p^2}{y^2}\right)\cdot exp\left(-\beta^2\cdot\frac{L^2\cdot v_p^2}{y^2}\right)\right] \qquad (8)$$

However, for evaluating the depletion effect on ablation rate quantitatively it is necessary to make calculations of the heat transfer through the neutral gas cloud and average the deflection factor D over the pellet surface.

It is clear that the depletion deals only with the electron part of the heat flow onto the pellet because the ion flux comes from the radial directions. For contemporary

machines the electron flow can be considered as collisionless everywhere.

The heat flux penetrating through the neutral gas with the line density integral or "optical thickness" Sn is defined by formula

$$Q_e(Sn)=\frac{2}{m_e^{1/2}\cdot\pi^{1/2}}\int_0^1\int_0^\infty E^2\cdot nf(E,z,Sn)\cdot z\cdot dEdz \tag{9}$$

$$f(E,z,Sn)=\left(\frac{Eo}{E}\right)^{1/2}\cdot\frac{Le(Eo)}{Le(E)}\cdot exp\left(-\frac{Eo}{T_e}\right) \tag{10}$$

$$Eo(E,z,Sn)=-586+\left[586^2+\frac{1}{2\cdot10^{11}}\left(\frac{Sn}{z}+2.35\cdot10^{14}\cdot E+2\cdot10^{11}\cdot E^2\right)\right]^{1/2} \tag{11}$$

$$Le(E)=\left(2.35\cdot10^{14}+4\cdot10^{11}\cdot E\right)^{-1} \tag{12}$$

Here Eo and E are the energies at the cloud border and at the pellet surface correspondingly, z is the cosine of the electron pitch angle relative to the magnetic field, $Le(E)$ is the energy loss function (see Ref. [10] for details).

To account for the modifications of the distribution function due to depletion it is sufficient to add the Heaviside step function H into the integral (9)

$$Q_e(Sn,y)=\frac{2}{m_e^{1/2}\cdot\pi^{1/2}}\int_0^1\int_0^\infty E^2\cdot nf(E,z,Sn)\cdot z\cdot H\left(L-\sqrt{\frac{2\cdot E}{m_e}}\cdot\frac{y}{v_p}\cdot z\right)dEdz \tag{13}$$

This integral obviously becomes equal to Eq. (9) for $L=\infty$ supreme or $y=0$.

The local ablation rate density can be determined using gas dynamic scaling for the cloud [11,12]

$$\Gamma_s=0.383\cdot\left[\frac{5}{2}\cdot\frac{\gamma-1}{m_i}\cdot Qe(0)\cdot\left(\frac{Sn}{r_p}\right)^2\right]^{1/3} \tag{14}$$

when m_i is the pellet molecular mass, γ is the specific heat ratio for the pellet material.

The balance point between the energy flux onto the pellet surface and the sublimation energy flux at $Sn=Sn^*$ defines the local ablation rate.

$$Q_e(Sn^*)=\varepsilon\cdot\Gamma_s(Sn^*) \tag{15}$$

Owing the local ablation rate that depends both on the surface angle α and the poloidal angle φ, it is necessary to average the ablation rate over the pellet surface.

For this we should define the y value as the function of α and φ. Figure 2 shows the coordinate system used in the averaging procedure. The shadow distance y is defined by the following expression:

$$y(\alpha,\varphi)=r_p\cdot\left[\left(cos(\alpha)^2+sin(\alpha)^2\cdot cos(\varphi)^2\right)^{1/2}-sin(\alpha)cos(\varphi)\right] \tag{16}$$

After that the average ablation rate for the pellet is

$$\frac{dN}{dt}=\frac{2}{\varepsilon}\cdot\int_0^{\frac{\pi}{2}}\int_0^{2\pi}Q_e(Sn^*,y)\cdot cos(\alpha)\cdot sin(\alpha)d\alpha d\varphi \tag{17}$$

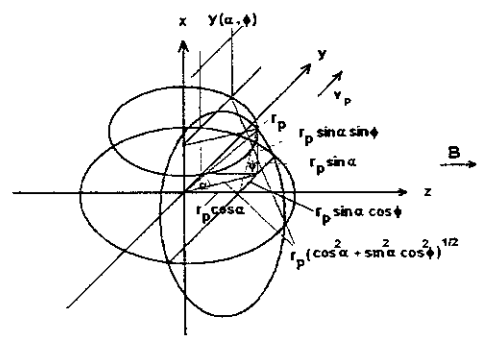

Fig. 2: Coordinate system for the averaging procedure.

3 Application of the Model to the T-10 Conditions

Let us consider the depletion effect in the T-10 conditions: R=150 cm, L=1000 cm, r_p=0.05 cm, v_p=500 m/s, T_e=500 eV, n_e=10^{13} cm^{-3}.

Figure 3 shows decay of the electron energy flux (Eq. (13)) versus the optical thickness of gas cloud for different shadow distances y.

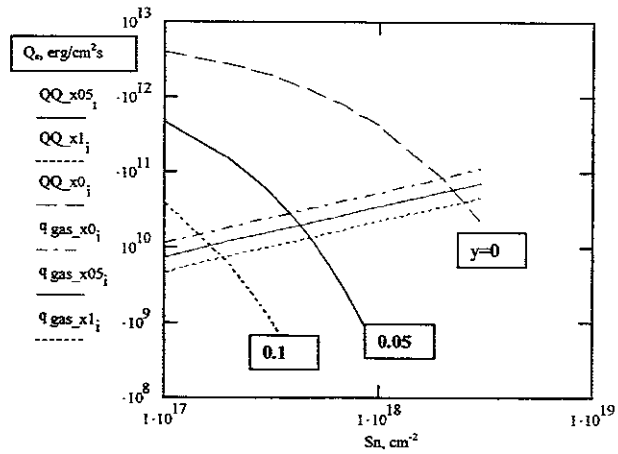

Figure 3: Electron heat flux and sublimation energy flux versus the cloud optical thickness for different shadow distances y=0, 0.05,0.1 cm.

It is clearly seen that the average energy of the flux decreases with the shadow distance. At the same figure the corresponding gas energy flows (Eqs. (14), (15)) are shown. Reduction of the local ablation rate with the y-value (balance points between the gas energy flow and the electron heat flow) is almost exponential (see Fig. 4, 5).

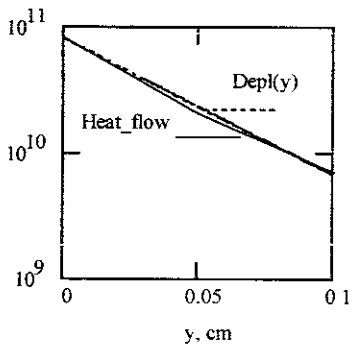

Figure 4: Heat flow $Q_e(y)$ versus shadow distance y and the approximating exponential dependence $Depl(y)$.

Approximating dependence for the depletion factor $D(y)$ being equal to

$$D(y)=\frac{Qe(y)}{Qe(0)}=exp\left(-\frac{y}{0.04}\right) \qquad (18)$$

fairly well describes the calculated points, which significantly simplifies the following averaging integration.

Following to Eq. (17) we get for the ablation rate reduction by a factor of 2.5.

It should be noticed that although the value of ablation rate reduction is not very large, the ablation rate is distributed over the pellet surface non-uniformly. This might produce a huge deceleration effect on the pellet passing a rational magnetic surface.

The deceleration value can be estimated as momentum transferred to the pellet from the ablated cloud. As the local ablation rate is known the particle flux multiplied by molecular mass immediately gives the normal pressure

$$P(\alpha,\varphi)=m_i\cdot U\cdot\Gamma(\alpha,\varphi) \qquad (19)$$

Averaging the projection of this pressure on the y-axis gives the force F acting on the pellet

$$F=2\cdot\frac{Q(Sn^*,0)}{\varepsilon}\cdot m_i\cdot U\cdot r_p^2\int_0^{\frac{\pi}{2}}cos(\alpha)\cdot sin^2(\alpha)\int_0^{\pi}D(y(\alpha,\varphi))\cdot cos(\varphi)d\varphi d\alpha$$

$$U=86.6\cdot r_p^{1/3}\cdot n_e^{1/3}\cdot T_e^{-0.07} \qquad (20)$$

The force F=6.87 kdin directed outward plasmas produces acceleration of the pellet equal to $4.1\cdot10^8$ cm/s^2. For the region with zero magnetic field shear, the losses of pellet velocity will be as large as 82 m/s per centimeter (~16.5%). The effect should be seen in experiments near magnetic islands where a rational number q region of centimeter spatial scale having a low shear is possible.

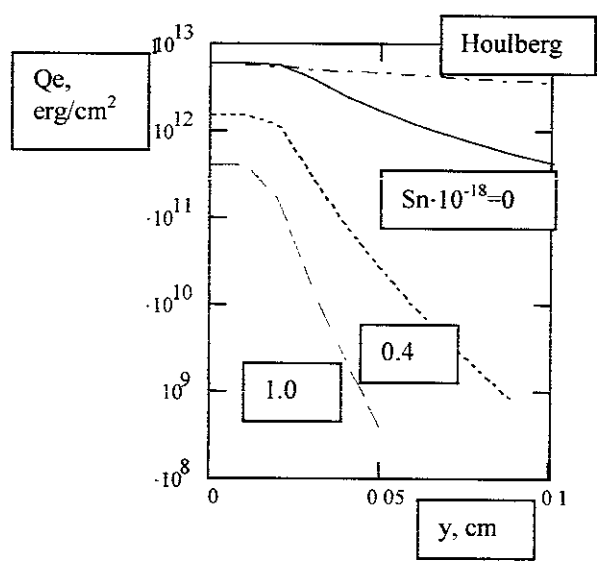

Figure 5: Variation of the electron heat flux with the shadow distance after penetration through the cloud with different distance Sn=0, 0.4, 1 $10^{18}\times$cm^{-2}. The Houlberg dependence

for Sn=0 is also shown. It is evident that the Houlberg dependence is significantly slower.

4 Toroidal Effects on Ablation

Injection of pellets from high field side is widely considered now as a way of deeper fuel delivery [13]. Experiments on ASDEX-Upgrade [14] and JET[15] have shown that pellet penetration is also deeper for the HFS injection. The ideas about additional shielding of the pellet by the plasma cloud moving ahead due toroidal shift were offered as a possible explanation of this deeper penetration at a qualitative level. However, until now there were no quantitative evaluations of the ablation rate in toroidal systems. Below this situation is considered. Effects of the toroidal geometry on the electron ablating heat fluxes for LFS and HFS are presented.

Before the analysis of the problem it should be noticed that in tokamaks the magnetic surfaces are shifted outward due to Shafranov shift [16]. Accordingly, the gradients for the low field side are higher and lower for the HFS. This effect is clearly seen in Fig. 3.3.1 of the Wesson "Tokamaks" [16]. Near plasma border the difference between the HFS and LFS gradients is about 2 times becoming negligible in the central zone.

A typical Shafranov shift for ASDEX Upgrade (R=150 cm, a=50 cm, l_i=1.4, β_p=1) is

$$\Delta = 0.6 \cdot \frac{a^2}{R} = 10 \text{ cm} \qquad (21)$$

Assuming that the density gradient and temperature gradient deposit equally into the pressure we can evaluate penetration of the pellet for normal gradient and that reduced by a factor of 2. The results are presented in the Table 1. The gradients assumed correspond to ITER parameters but they correlate with contemporary machines as well.

Table 1.

r_p, cm	dn_e/dr, dT_e/dr $20\cdot10^{13}$ cm^{-3} per 280 cm; 14000 eV per 280 cm HFS	dn_e/dr, dT_e/dr $28\cdot10^{13}$ cm^{-3} per 280 cm; 20000 eV per 280 cm LFS	Penetration Ratio HFS/HFS
0.5	80	62.5	1.28
0.1	33	26.5	1.29

We see that, although the penetration depth is longer for the HFS case, the pellet still does not reach the same pressure level (1.29<2) as the LFS case gives. This means that at least for the fueling the LFS injection gives advantages due to the profile effect.

Analyzing the modification of electron distribution function due to the influence of the magnetic field decrease with the major radius let us assume that the electrons come from the extreme magnetic field points. For the LFS injection this is the point with maximal magnetic field, while for the HFS this is the point with the lowest magnetic field. At these points placed at the distance equal to $L=\pi\ R\cdot q$ the distributions are assumed to be Maxwellian

Since the magnetic field varies with the major radius as $1/R$, the transverse energy reduces in collisionless LFS case. During electron flight to the pellet cloud the tilt angle decreases in average For the HFS case the tilt angle increases, and the magnetic mirror reflects a part of electrons

These two factors: Shafranov shift and the mirrors effect; provide larger ablation for the low field side and the lower ablation in the HFS case.

Fig. 6 shows the modification of tilt angle cosine for the case of LFS injection at different aspect ratios on the magnetic surface.

$$z_{new}^{LFS} = \left[1 - \left(1 - z^2\right) \cdot \left(\frac{R-r}{R+r}\right)\right]^{1/2} \qquad (22)$$

It is seen that electrons with small longitudinal energy (z=0) decrease the tilt angle and the effect is larger near the plasma border being also significant in middle zone of the minor radius. For r/R=35/150 the maximal angle is 52 degrees. So, the orientation of the flow along the magnetic field line is evident.

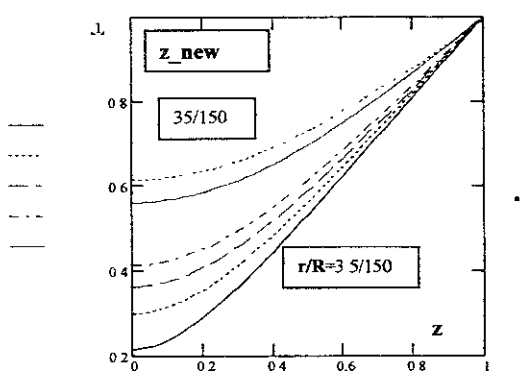

Figure 6: Dependence of the $z_{new}=cos(\theta)$ at the pellet cloud border versus the initial z-value for different aspect ratios. (LFS-case).

On the other hand, the behavior of the distribution function for the HFS case is different. Only electrons with the tilt angle less than a definite value enable to reach the cloud surface. Fig. 7 shows the corresponding dependencies of the tilt angle at the cloud border versus the initial tilt angle cosine for different aspect ratios.

$$z_{new}^{HFS} = \left[1 - \left(1 - z^2\right) \cdot \left(\frac{R+r}{R-r}\right)\right]^{1/2} \qquad (23)$$

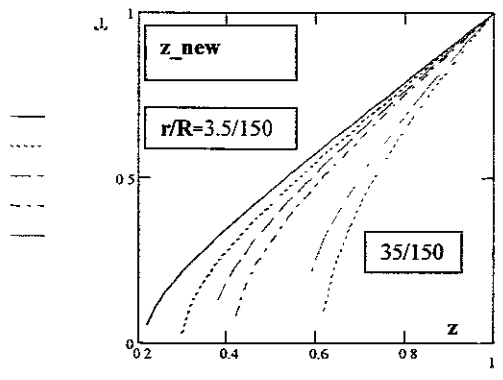

Figure 7: Dependence of the $z_{new}=cos(\theta)$ at the pellet cloud border versus the initial z-value for different aspect ratios. (HFS-case).

As it is seen (and well know [16]), the amount of trapped particles, which are reflected, is rather large. So, even for a moderate aspect ratio ~5 the majority of electrons is reflected from the magnetic mirror. Only electrons with tilt angle less than 58 degrees can reach he cloud at this aspect ratio.

The distribution over the tilt angle cosine (being equal to unity for the Maxwellian distribution function) undergoes significant changes.

$$\frac{dz}{dz_{new}^{LFS}} = \frac{z_{new}^{LFS} \cdot (R+r)}{\left[(R-r) \cdot \left((R+r) \cdot z_{new}^{LFS\,2} - 2 \cdot r\right)\right]^{1/2}}$$

$$\frac{dz}{dz_{new}^{HFS}} = \frac{z_{new}^{HFS} \cdot (R-r)}{\left[(R+r) \cdot \left((R-r) \cdot z_{new}^{HFS\,2} + 2 \cdot r\right)\right]^{1/2}} \qquad (24)$$

Figure 8 shows the initial distribution and two others. It should be noticed that for LFS injection the integral over the distribution is equal to unity as in the isotropy case. For the HFS the integral is lower than unity by a factor of 2.5 (at r/R~5).

Integration over distribution functions for LFS and HFS gives the corresponding reduction of the energy flow with the cloud optical length.

$$Q_e(Sn) = \frac{2}{m_e^{1/2} \cdot \pi^{1/2}} \int_{z_{new}^{min}}^{1} \int_{0}^{\infty} E^2 \cdot nf\left(E, z_{new}, Sn\right) \cdot \frac{dz}{dz_{new}} \cdot z_{new} \cdot dE dz_{new} \qquad (25)$$

Here, the minimal z_{new} is equal to zero for the HFS injection and

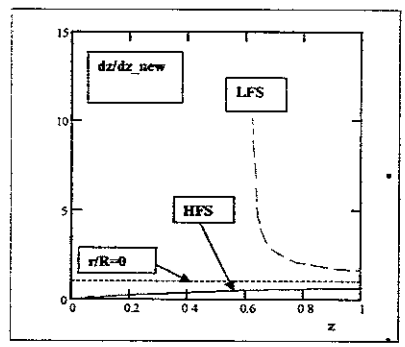

Figure 8: Distribution of electrons over $cos(\theta)$ for isotropy Maxwellian function, LFS and HFS injections.

$$z_{new}^{min} = \left[\frac{2 \cdot r}{R+r}\right]^{1/2} \qquad (26)$$

for the LFS one.

Figure 9 shows heat flows for the cases considered along with the corresponding to the zero-Sn condition ablation heat flows. The lines mark corresponding balance points.

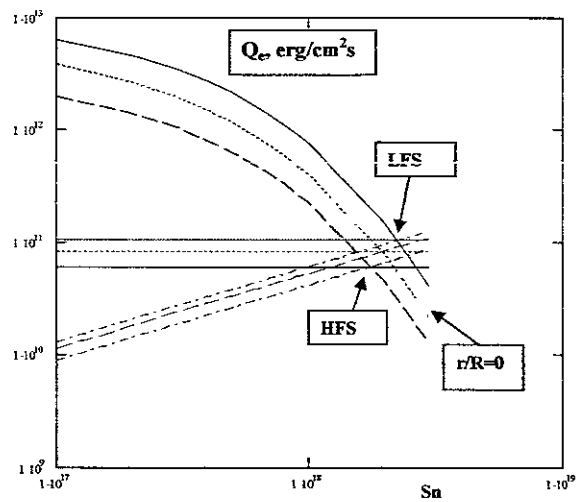

Figure 9: Electron and ablation heat flows for LFS, HFS and uniform magnetic field cases.

We see that compared with the uniform magnetic field, the ablation rate is higher for the LFS injection by a factor of 1.28 and lower for the HFS by a factor of 0.73. Thus, the ratio of the ablation rates for the HFS to LFS is about 1.75. The effect of such difference is comparable with that of the Shafranov shift. The difference in the penetration length is presented in Table 2.

Table 2

r_p, cm	dn_e/dr, dT_e/dr $20 \cdot 10^{13}$ cm^{-3} per 280 cm 14000 eV per 280 cm HFS	dn_e/dr, dT_e/dr $28 \cdot 10^{13}$ cm^{-3} per 280 cm 20000 eV per 280 cm LFS	Penetration Ratio HFS/HFS
0.5	88	58	1.5
0.1	36	24	1.5

The penetration depth for the HFS injection becomes 1.5 times longer than for the LFS. However, the fueling efficiency for the HFS is still better because the pellet from HFS reaches the zone with 1.4 times higher pressure.

5 Summary

A kinetic depletion model is developed. The depletion parameters can be evaluated quantitatively using the model. The correlation with experiments is evident.

A new three-dimensional effect is detected. This is pellet deceleration in the vicinity of rational magnetic surfaces. The pellet trajectory is significantly affected by this factor. For stellarators with q=1 island near the border the effect can be significant for penetration.

Penetration from LFS and HFS into toroidal machines is affected by two comparable factors. Those are Sharanov shift of the magnetic surfaces, which reduces the pressure gradient at the HFS (in tokamaks). It yields about 30 % deeper penetration for HFS injection. About the same effect is produced by the modification of the electron distribution function by the toroidal magnetic field. The total effect on the penetration ration about 1.5 is possible. This should be accounted for first when additional drift effects on the particle deposition are considered.

Acknowledgements

The author is grateful to Prof. L.D. Tsendin and Prof. Sudo for their attention to the work and fruitful discussions. The work was fulfilled under the contract with NIFS.

References

[1] W.A. Houlberg et al., Nuclear Fusion **28** (1988) 595.

[2] B. Pegourie, M.A. Dubois, Nuclear Fusion 29 (1989) 745.

[3] B. Pegourie, M.A. Dubois, Nuclear Fusion 30 (1990) 1575.

[4] S.C. McCool et al., Europhysics Conference Abstracts Vol. 15C, Part I, (1991) p. 325

[5] S.L. Milora et al. Nuclear Fusion **35** (1995) 657.

[6] L. R. Baylor et al., Nuclear Fusion **31** (1991) 1249.

[7] S.L. Milora et al. Nuclear Fusion **20** (1980) 1491.

[8] B.V. Kuteev et al, Plasma Physics Reports **11** (1985) 236.

[9] G.A. Bird, Molecular Gas Dynamics, Claredon Press, Oxford, 1976.

[10] B.V. Kuteev, Nuclear Fusion **35** (1995) 431.

[11] B.V. Kuteev, L.D. Tsendin, et al. Fusion Technology **26** (1994) 938.

[12] B.V. Kuteev, L.D. Tsendin. Report NIFS 2001, Analitical Model of Neutral Gas Shielding for Hydrogen Pellet Ablation .

[13] P.T. Lang et al, Phys. Rev. Letters, **79** (1997) 1487.

[14] P.T. Lang et al. EPS-2001, Madeira. Performance improvement by advanced high field side pellet refueling in ASDEX-Apgrade.

[15] P.T. Lang et al. EPS-2001, Madeira. Optimization scenarios for long pulse fueling to high densities at JET.

[16] J. Wesson. Tokamaks, Clarendon Press-Oxford, 1997.

Recent Issues of NIFS Series

NIFS-691 A Yoshizawa, S -I Itoh, K Itoh and N Yokoi,
Turbulence Theories and Modelling of Fluids and Plasmas Apr 2001

NIFS-692 K Ichiguchi, T Nishimura, N Nakajima, M Okamoto S -i Oikawa M Itagaki,
Effects of Net Toroidal Current Profile on Mercier Criterion in Heliotron Plasma Apr 2001

NIFS-693 W Pei, R Horiuchi and T Sato,
Long Time Scale Evolution of Collisionless Driven Reconnection in a Two-Dimensional Open System Apr 2001

NIFS-694 L N Vyacheslavov, K Tanaka, K Kawahata,
CO2 Laser Diagnostics for Measurements of the Plasma Density Profile and Plasma Density Fluctuations on LHD Apr 2001

NIFS-695 T Ohkawa,
Spin Dependent Transport in Magnetically Confined Plasma May 2001

NIFS-696 M Yokoyama, K Ida, H Sanuki, K Itoh, K Narihara K Tanaka, K Kawahata, N Ohyabu and LHD experimental group
Analysis of Radial Electric Field in LHD towards Improved Confinement. May 2001

NIFS-697 M Yokoyama, K Itoh, S Okamura, K Matsuoka, S -I Itoh,
Maximum-J Capability in a Quasi-Axisymmetric Stellarator May 2001

NIFS-698 S-I Itoh and K Itoh,
Transition in Multiple-scale-lengths Turbulence in Plasmas May 2001

NIFS-699 K Ohi, H. Naitou, Y Tauchi, O Fukumasa,
Bifurcation in Asymmetric Plasma Divided by a Magnetic Filter May 2001

NIFS-700 H Miura, T Hayashi and T Sato,
Nonlinear Simulation of Resistive Ballooning Modes in Large Helical Device· June 2001

NIFS-701 G Kawahara and S Kida,
A Periodic Motion Embedded in Plane Couette Turbulence June 2001

NIFS-702 K Ohkubo,
Hybrid Modes in a Square Corrugated Waveguide June 2001

NIFS-703 S -I Itoh and K. Itoh,
Statistical Theory and Transition in Multiple-scale-lengths Turbulence in Plasmas June 2001

NIFS-704 S. Toda and K Itoh,
Theoretical Study of Structure of Electric Field in Helical Toroidal Plasmas June 2001

NIFS-705 K. Itoh and S-I Itoh,
Geometry Changes Transient Transport in Plasmas June 2001

NIFS-706 M Tanaka and A Yu Grosberg
Electrophoresis of Charge Inverted Macroion Complex· Molecular Dynamics Study July 2001

NIFS-707 T-H Watanave, H Sugama and T Sato
A Nondissipative Simulation Method for the Drift Kinetic Equation July 2001

NIFS-708 N Ishihara and S Kida,
Dynamo Mechanism in a Rotating Spherical Shell Competition between Magnetic Field and Convection Vortices July 2001

NIFS-709 LHD Experimental Group,
Contributions to 28th European Physical Society Conference on Controlled Fusion and Plasma Physics (Madeira Tecnopolo, Funchal, Portugal, 18-22 June 2001) from LHD Experiment July 2001

NIFS-710 V Yu. Sergeev, R.K Janev, M.J. Rakovic, S Zou. N Tamura, K V Khlopenkov and S Sudo
Optimization of the Visible CXRS Measurements of TESPEL Diagnostics in LHD, Aug 2001

NIFS-711 M Bacal, M. Nishiura, M. Sasao, M Wada, M Hamabe, H Yamaoka,
Effect of Argon Additive in Negative Hydrogen Ion Sources, Aug 2001

NIFS-712 K Saito, R Kumazawa, T Mutoh T Seki, T Watari, T Yamamoto, Y Torii, N Takeuchi C Zhang, Y. Zhao, A Fukuyama, F Shimpo, G Nomura, M Yokota, A Kato M Sasao, M Isobe, A V Krasilnikov, T Ozaki, M. Osakabe, K Narihara, Y Nagayama, S Inagaki, K Itoh, T Ido S Morita K Ohkubo M Sato S Kubo, T Shimozuma H Idei Y Yoshimura, T Notake, O Kaneko, Y Takeiri, Y. Oka, K Tsumori, K. Ikeda, A. Komori, H Yamada, H Funaba. K Y Watanabe, S Sakakibara, R Sakamoto, J. Miyazawa, K Tanaka B J Peterson, N Ashikawa, S Murakami, T Minami, M Shoji, S Ohdachi, S Yamamoto, H. Suzuki, K. Kawahata, M Emoto, H Nakanishi, N Inoue, N Ohyabu, Y Nakamura, S Masuzaki, S Muto, K Sato, T Morisaki, M Yokoyama, T Watanabe, M Goto, I. Yamada, K Ida, T Tokuzawa, N Noda, K Toi, S Yamaguchi, K Akaishi, A. Sagara, K Nishimura, K Yamazaki, S Sudo, Y Hamada, O Motojima, M Fujiwara,
A Study of High-Energy Ions Produced by ICRF Heating in LHD Sep 2001

NIFS-713 Y Matsumoto, S -I Oikawa and T Watanabe,
Field Line and Particle Orbit Analysis in the Periphery of the Large Helical Device, Sep 2001

NIFS-714 S Toda, M Kawasaki, N Kasuya, K Itoh, Y Takase, A Furuya, M Yagi and S -I Itoh,
Contributions to the 8th IAEA Technical Committee Meeting on H-Mode Physics and Transport Barriers (5-7 September 2001, Toki, Japan) Oct 2001

NIFS-715 A Maluckov, N. Nakajima, M. Okamoto, S Murakami and R Kanno,
Statistical Properties of the Particle Radial Diffusion in a Radially Bounded Irregular Magnetic Field, Oct 2001

NIFS-716 Boris V Kuteev,
Kinetic Depletion Model for Pellet Ablation, Nov 2001